

SUPPORTING INFORMATION

Local Mechanical Properties of Electrospun Fibers

Correlate to Their Internal Nanostructure

Andrea Camposeo,^{,†,‡,□} Israel Greenfeld,^{*,§,□} Francesco Tantussi,^{||,⊥} Stefano Pagliara,^{†,■} Maria
Moffa,^{†,‡} Francesco Fuso,^{||,⊥} Maria Allegrini,^{||,⊥} Eyal Zussman,[§] Dario Pisignano,^{*,†,‡,¶}*

[†]National Nanotechnology Laboratory of Istituto Nanoscienze-CNR, via Arnesano, I-73100
Lecce (Italy)

[‡]Center for Biomolecular Nanotechnologies @UNILE, Istituto Italiano di Tecnologia, via
Barsanti, I-73010 Arnesano, LE (Italy)

[§]Department of Mechanical Engineering, Technion - Israel Institute of Technology, Haifa 32000,
Israel

^{||}Dipartimento di Fisica “Enrico Fermi” and CNISM, Università di Pisa, Largo Bruno
Pontecorvo 3, I-56127 Pisa (Italy)

[⊥]Istituto Nazionale di Ottica INO-CNR, Sezione di Pisa, I-56127 Pisa (Italy)

[¶]Dipartimento di Matematica e Fisica “Ennio De Giorgi”, Università del Salento, via Arnesano
I-73100 Lecce, (Italy)

1. Nanofiber Morphology

Figure S1 displays the MEH-PPV fiber morphology as obtained by scanning electron microscopy (SEM) and atomic force microscopy (AFM). SEM analysis is performed by using a Nova NanoSEM 450 field emission system (FEI) operating with an acceleration voltage of 5 kV and an aperture size of 30 μm . A thin layer of Cr (<10 nm) is thermally evaporated on top of the samples before SEM imaging. Figures S1a,b display the SEM images of MEH-PPV fibers deposited on quartz substrates and then analysed by near-field optical analysis. The fibers have mean diameters of about 500 nm.

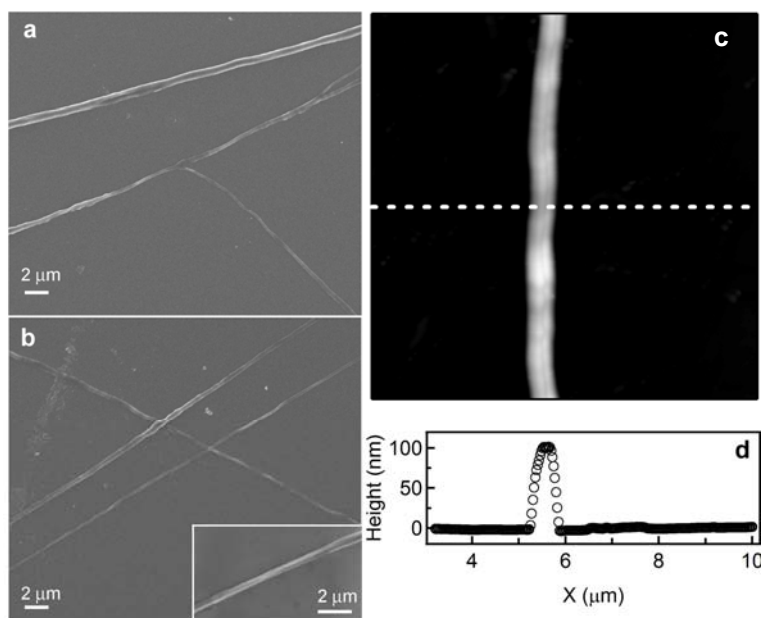


Figure S1. (a, b) SEM images of MEH-PPV fibers. (c, d) AFM topographic map (c) and height profile (d) of a MEH-PPV fiber (width 450 nm and height 100 nm.).

The surface topography of the nanofibers is investigated by AFM, employing a Multimode head (Veeco Instruments, Plainview, NY) equipped with a Nanoscope IIIa controller and

operating in tapping mode. Phosphorous-doped Si tips are employed, with an 8-10 nm nominal curvature radius and a resonant frequency of 250 kHz. Figures S1c,d display a typical AFM topography map of a MEH-PPV fiber, evidencing a ribbon-shape. Similar results are obtained by measuring the fiber topography by the shear-force method with the scanning near field optical microscope (Fig. S2).

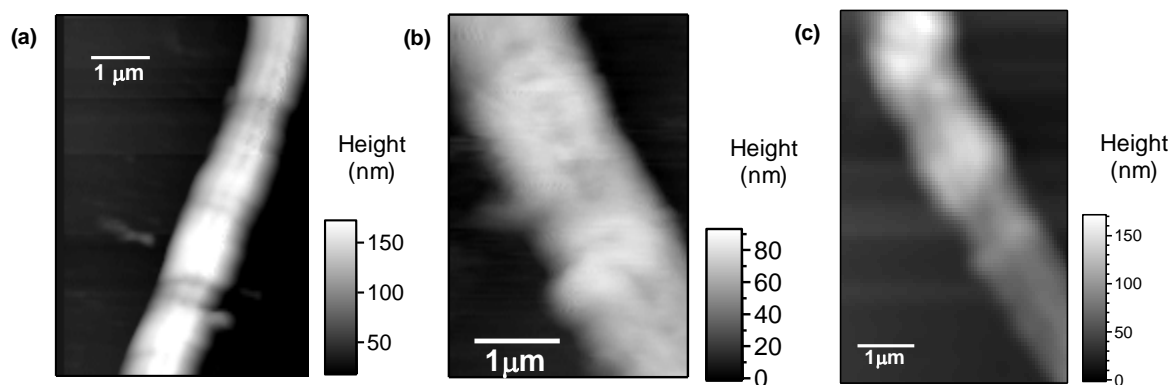


Figure S2. Examples of topography maps of MEH-PPV fibers obtained by the shear-force method. The map reported in (a) corresponds to the topography of the fiber displayed in Fig. 3. The fiber height is < 170 nm, whereas the width is about $1 \mu\text{m}$, in accordance with the ribbon shape of the fiber evidenced by both AFM and SEM measurements (Fig. S1).

2. Force-Indentation measurements.

The nanoscale spatial variation of the nanofiber elastic modulus is measured by acquiring force (F_{load}) vs distance curves, by using a Multimode AFM system equipped with a Nanoscope IIIa electronic controller (Veeco Instruments). The force vs. distance curves are then converted in force vs. deformation plots (F_{load} vs. δ).^{S1,S2} The dependence of the applied load on the deformation of the sample (δ) is approximated by the Hertz model:^{S3}

$$F_{load} = \left(\frac{4}{3} \sqrt{R} \right) \left(\frac{1 - \nu_t^2}{E_t} + \frac{1 - \nu_{fiber}^2}{E_{fiber}} \right)^{-1} \delta^{\frac{3}{2}} \quad (S1)$$

where R is the tip radius, ν_t and ν_f are the Poisson's ratio of the cantilever ($\nu_t = 0.27$) and of the fiber ($\nu_f = 0.35$), respectively, and E_t and E_{fiber} are the Young's modulus of the cantilever ($E_t = 160$ GPa) and of the nanofiber, respectively. The nanofiber Young's modulus is obtained by fitting the force vs. indentation curves to Eq. S1.^{S4}

Indentation measurements on the surface of fibers (Fig. S3) are performed by applying the load, F_{load} , along a direction perpendicular to the quartz substrate and to the fiber longitudinal axis, assuring the absence of bending or buckling of the fiber during the measurement. Indeed, AFM images of the investigated region, acquired before and after indentation measurements, do not evidence variations of the fiber morphology and position. Due to the finite thickness of the fiber deposited on the quartz substrate, these measurements can be affected by the presence of the stiffer substrate. B. Cappella *et al.*^{S5} have reported a dependence of the measured effective elastic modulus on the thickness of the polymer film deposited on glass. In particular they have observed an increase of the effective elastic modulus *upon decreasing* the film thickness, since for thinner films the indentation measurement is sensitive also to the mechanical properties of the substrate.

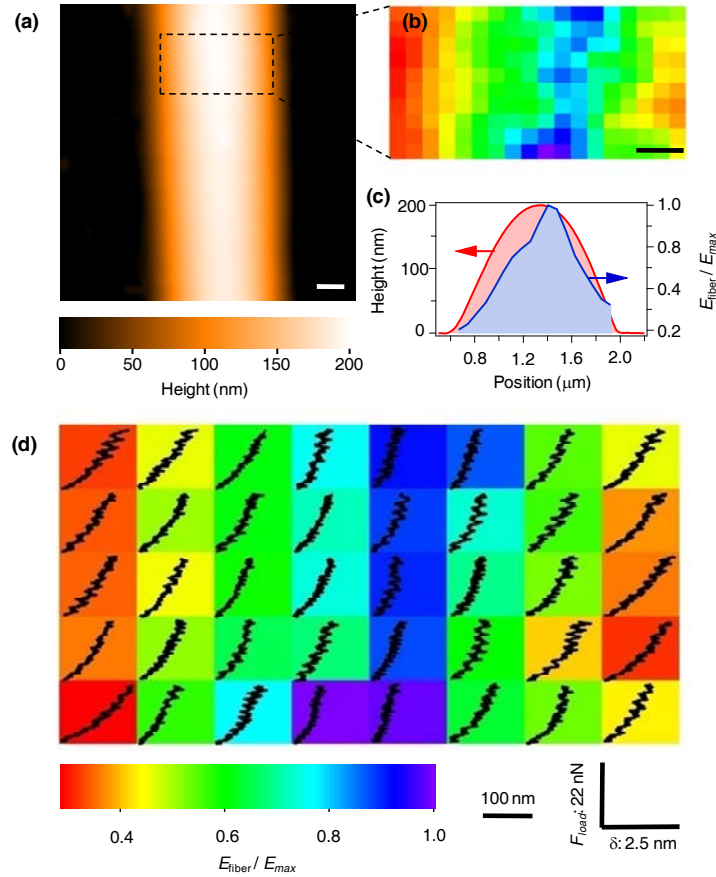


Figure S3. (a) AFM micrograph of a single MEH-PPV spun fiber. Scale bar: 250 nm. (b) Corresponding Young's modulus (E_{fiber}) map, normalized to the maximum value (E_{max}). Scale bar: 200 nm, color scale shown in the bottom of the Figure. The map is obtained by determining the force-distance curves in the region highlighted by a dashed box in (a). (c) Line profiles showing the cross-sections of the topography (red continuous line) and of E_{fiber} (blue continuous line). (d) Example of applied load (F_{load}) vs. deformation (δ) curves measured in different points of the fiber surface. Each pixel area is $140 \times 140 \text{ nm}^2$, and the pixel color shows the local normalized Young's modulus. The curves shown in each pixel have higher slopes for stiffer regions, according to (x, y) axes (δ and F_{load}), respectively, shown in the bottom-right corner. The overall analyzed area is highlighted in (a) by a dashed box.

They also proposed a semi-empirical analysis that allows to obtain the mechanical properties of the polymer film, taking into account its finite thickness.^{S6} The force-distance measurements performed on a fiber deposited on quartz substrate provide therefore an effective elastic modulus, possibly affected by the substrate. In particular, for a fiber composed by uniformly distributed polymer, *larger* effective values are expected at the fiber border, due to the reduced thickness and to the relatively major contribution from the substrate. Instead, we find a *decrease* of the elastic modulus at the fiber border (Fig. S3), that can be related to the presence of a softer fiber sheath, as confirmed by the fiber cross-section measurements discussed in the main paper (Fig. 2). In Fig. S4, two examples of force vs. indentation (δ) curves, measured at the fiber core and sheath, respectively, are shown.

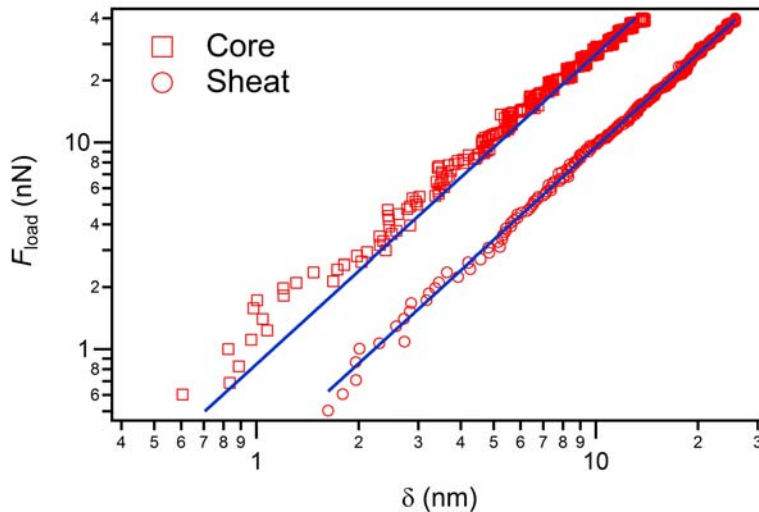


Figure S4. Examples of force vs. indentation (δ) curves measured on the fiber cross-section surface in the core (squares) and sheath (circles). The difference of the resulting E_{fiber} is evidenced by the different intercepts of the curves with the F_{load} axis in the bi-logarithmic plot. The continuous lines are fits to the data by Eq. S1.

3. SNOM measurements

The spatial variation of the polymer density in the fibers is evaluated by near-field absorption microscopy, a measurement allowing to estimate the absorption coefficient, that depends on the local density of the absorbing chromophores, according to the Lambert-Beer law. In order to obtain maps of the absorption coefficient (α), the light transmitted through the fiber illuminated by the optical near field of a tapered fiber is measured simultaneously to its topography. This is accomplished by the shear-force method,^{S7} allowing both the fiber-sample distance to be kept constant and the fiber height profile to be obtained in each scan. Examples of fiber topography maps obtained by this method are shown in Fig. S2. The map of the absorption coefficient is then calculated as: $\alpha(x, y) = -\ln[T(x, y)]/h(x, y)$, where $T(x,y)$ is the map of the fiber transmission coefficient and $h(x,y)$ is the local, measured fiber thickness, which is fully taken into account in this way. Examples of transmittance and absorption coefficient maps obtained in various MEH-PPV fibers are shown in Fig. S5.

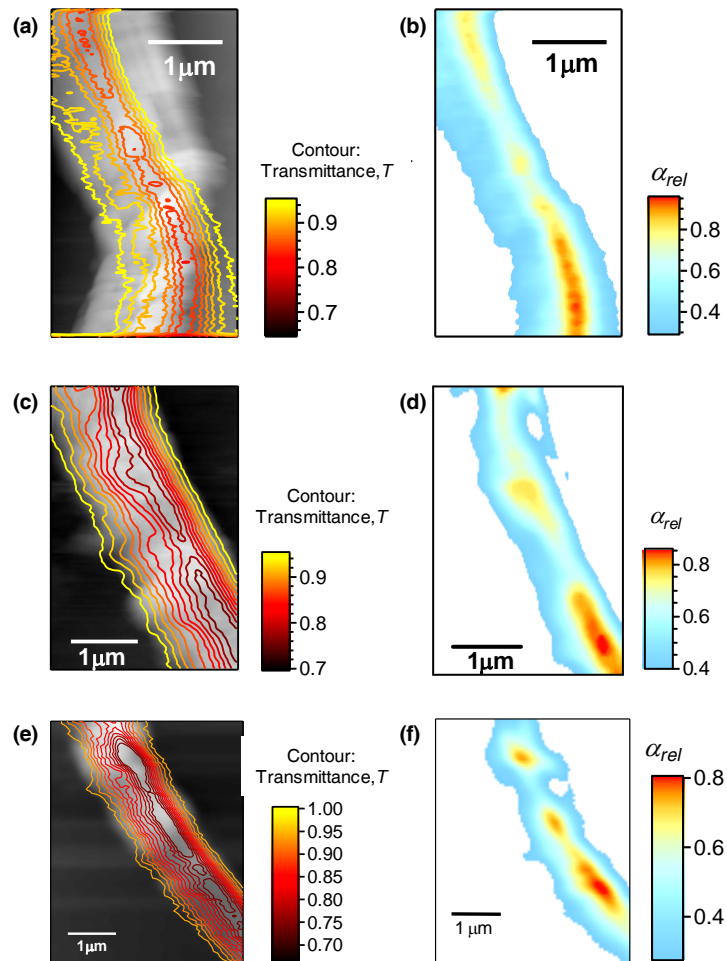


Figure S5. (a, c, e) Examples of fiber topography maps, with superimposed contour plots of the SNOM transmission data, and corresponding maps of the nanoscale variation of optical absorption (b, d, f) respectively.

References.

- S1. Tan, S.; Sherman Jr., R. L.; Ford, W. T. Nanoscale compression of polymer microspheres by atomic force microscopy. *Langmuir* **2004**, *20*, 7015-7020.
- S2. Touhami, A.; Nysten, B.; Dufrene, Y. F. Nanoscale mapping of the elasticity of microbial cells by atomic force microscopy. *Langmuir* **2003**, *19*, 4539-4543.

- S3. Butt, H. J.; Cappella, B.; Kappl, M. Force measurements with the atomic force microscope: technique, interpretation and applications. *Surf. Sci. Rep.* **2005**, *59*, 1-152.
- S4. Lin, H.-N. ; Lin, H.-L.; Wang, S.-S.; Yu, L.-S.; Perng, G.-Y.; Chen, S.-A.; Chen, S.-H. Nanoscale charge transport in an electroluminescent polymer investigated by conducting atomic force microscopy. *Appl. Phys. Lett.* **2002**, *81*, 2572.
- S5. Cappella, B.; Silbernagl, D. Nanomechanical properties of mechanical double layers: a novel semiempirical analysis. *Langmuir* **2007**, *23*, 10779-10787.
- S6. Silbernagl, D.; B. Cappella. Reconstruction of a ridge topography by single AFM force-distance curves. *Surf. Sci.* **2009**, *603*, 2363-2369.
- S7. Karrai, K.; Grober, R. D. Piezoelectric tip-sample distance control for near field optical microscopes. *Appl. Phys. Lett.* **1995**, *66*, 1842.